ISSN 0006-3509, Biophysics, 2011, Vol. 56, No. 2, pp. 304–308. © Pleiades Publishing, Inc., 2011.
Original Russian Text © A.G. Orlova, A.V. Maslennikova, G.Yu. Golubyatnikov, V.A. Kamenskii, N.M. Shakhova, A.A. Babaev, L.B. Snopova, I.P. Ivanova, V.I. Plekhanov, T.I. Pryanikova, I.V. Turchin, 2011, published in Biofizika, 2011, Vol. 56, No. 2, pp. 349–355.

COMPLEX SYSTEMS BIOPHYSICS

Noninvasive Estimation of the Oxygen Status of Experimental Tumors by Diffuse Optical Spectroscopy

A. G. Orlova[a], A. V. Maslennikova[a, b], G. Yu. Golubyatnikov[a], V. A. Kamensky[a], N. M. Shakhova[a], A. A. Babaev[c], L. B. Snopova[b], I. P. Ivanova[b], V. I. Plekhanov[a], T. I. Pryanikova[c], and I. V. Turchin[a]

[a] *Institute of Applied Physics, Russian Academy of Sciences, Nizhny Novgorod, 603950 Russia*
E-mail: orlova@ufp.appl.sci-nnov.ru
[b] *Nizhny Novgorod State Medical Academy, Nizhny Novgorod, Russia*
[c] *Lobachevsky State University, Nizhny Novgorod, Russia*

Received September 21, 2009; in final form, April 19, 2010

Abstract—The potentialities of diffuse optical spectroscopy for noninvasive estimation of the oxygen status of experimental tumors have been demonstrated. The distribution of total, oxygenated, and deoxygenated hemoglobin, as well as the level of oxygen saturation of blood have been assessed using two tumor models differing in the histological structure and functional characteristics. The results obtained by the optical method have been verified by immunohistochemical examination of tissue specimens with an exogenous hypoxia marker pimonidazole.

Keywords: tumor oxygen status, hypoxia, diffuse optical spectroscopy, noninvasive diagnosis, experimental tumors

DOI: 10.1134/S0006350911020230

INTRODUCTION

Hypoxia is a weighty factor of tumor progression and a source of resistance of the neoplasm to radio- and chemotherapy [1, 2]. The prognostic value of the partial oxygen tension has been proved clinically for cervical cancer, head and neck cancer, breast cancer, and soft-tissue sarcomata [3–6]. Better understanding of the role of hypoxia in clinical and experimental oncology has spurred the development of methods for assessing the tumor oxygen status. The most exact information is provided by direct polarographic measurement of pO_2, which is the "golden standard" in this field [7], but its clinical use is limited because the method is invasive. Immunohistochemical (IHC) methods, assaying exogenous or endogenous markers of hypoxia and affording a 2D map of hypoxic zones as well as an indication of relative oxygen content [8], are quite expensive and laborious, and besides that, are applicable only ex vivo.

The main techniques for in vivo assessment of the tumor oxygen status are magnetic resonance tomography and radionuclide ones (positron emission tomography and one-photon emission computer tomography) [9, 10]. An EPR-based method is currently developed [11]. In recent years, increasing recognition has been gained by noninvasive visualization techniques known as diffuse optical spectroscopy (DOS) [12, 13]. These methods consist in reconstructing the optical characteristics of biological tissues (scattering and absorption) from the data collected upon exposing the object to laser irradiation. With the spectroscopic data obtained at different wavelengths, one can infer the component analysis from the dispersion of absorption indices for the main tissue chromophores [total hemoglobin (tHb), oxyhemoglobin (HbO_2), deoxygenated or reduced hemoglobin (HHb), water, and lipids] and calculate the blood oxygenation level [14, 15]. DOS has been used for differential diagnosis of malignant and benign mammary neoplasms [16], for assessment of the metabolic status of the cancer and its dynamics during the course of chemotherapy [17, 18].

DOS is performed in different sounding configurations: the emitter and the receiver are positioned "for transmission" or "for reflection" to collect data for the entire volume or near the surface. Three-dimensional reconstruction is the task of diffuse optical tomography; because of heavy light scattering in tissue, it is not yet possible to attain a spatial resolution better than 6 mm even with a large number of emitters and receivers [19].

In this work, we aimed to design a noninvasive optical technique for estimating the oxygen status of experimental tumors and validate it in IHC assays with an exogenous marker of hypoxia, pimonidazole.

Abbreviations: DOS, diffuse optical spectroscopy; IHC, immunohistochemical; Pim, pimonidazole; PLS, Pliss lymphosarcoma; RMC, rat mammary cancer.

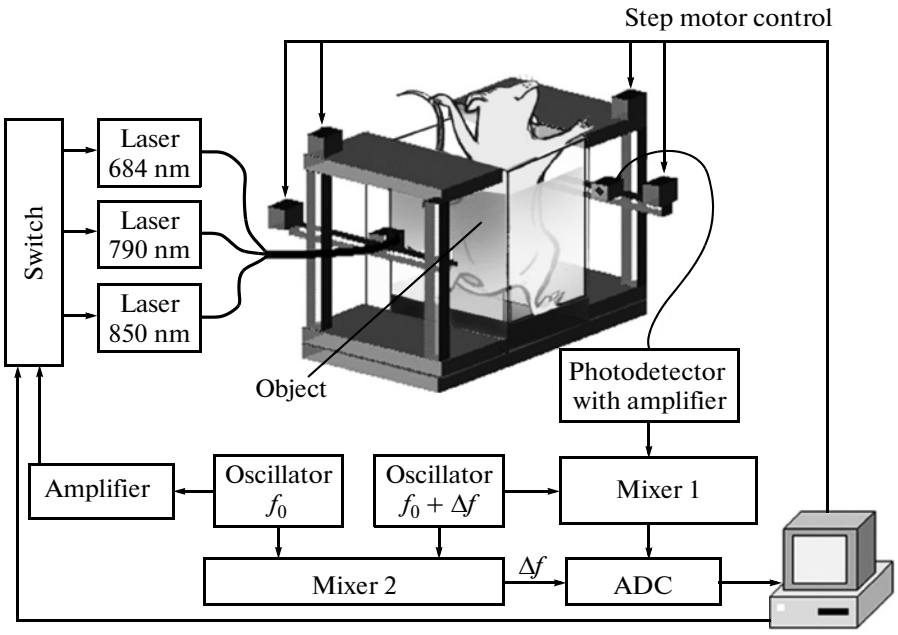

Fig. 1. Scheme of the DOS setup.

EXPERIMENTAL

Animals and tumor models. Experiments were performed on mongrel albino rats kept in standard vivarium conditions. The two tumor models were Pliss lymphosarcoma (PLS) and rat mammary cancer (RMC-1), differing essentially in histological structure and functional characteristics. Tumor strains were obtained from the Blokhin Cancer Research Center.

Pliss lymphosarcoma is a metastasizing connective tissue tumor [20]. The tumor is compact and consists of small and large irregularly shaped cellular elements with nuclei of varying shape and size. PLS tumors are marked by high mitotic activity and good vascularization. Small and large necrotic foci are encountered. In this study, PLS was grafted subcutaneously on the inner side of the thigh to five male rats (200–230 g). Animals were taken for examination when the tumor node grew to 20–30 mm (days 3–5 after grafting) and necrotic foci had formed therein.

Rat mammary cancer is a solid epithelial tumor consisting of polymorphic poorly differentiated cells. The stroma presents as thin layers of connective tissue with a modest amount of thin-walled "plethoric" vessels [21]. RMC-1 was grafted subcutaneously into the axillary region to six female rats (100–150 g). Animals were taken for examination when the tumor node grew to 10–30 mm (days 30–40 after grafting).

Diffuse optical spectroscopy. The DOS complex (Fig. 1) was designed in IAP (Nizhny Novgorod) [22]. For component analysis, laser scanning was performed at three wavelengths: 684 nm, the absorption maximum of reduced hemoglobin (HHb); 850 nm, the absorption maximum of oxyhemoglobin (HbO_2); and 794 nm where the HHb and HbO_2 extinction coefficients are the same (tHb). The high-frequency (140 MHz) modulation of laser light used in our device provides for higher accuracy owing to separate determination of absorbance and scattering.

Before the examination the animal was narcotized, hair was removed from the tumor zone, the animal was immobilized on a special frame and placed into the cuvette with immersion liquid. The latter—a 10% lipofundin suspension in water ($n = 1{,}33$) with addition of Indian ink [23, 24]—was close to animal tissue in its optical parameters: scattering coefficient 10–20 cm^{-1}, absorption coefficient 0.04–0.06 cm^{-1} at 790 nm. The optical path of the cuvette was 40 mm.

Scanning was performed by synchronously moving (in steps of 1–2 mm) the emitter and detector at the opposite sides of the object in the sagittal plane (Fig. 1). The signal acquisition time at each of the three wavelengths was ~100 ms. It took 20 to 40 min to obtain one image, depending on its size and the scanning step.

Pattern reconstruction for component analysis. For an object of known thickness R it is possible to determine the line-of-sight mean constants of decay β and propagation h of the photon density wave:

$$\beta = \sqrt{\frac{3\mu'_{s0}}{2}\left(\sqrt{\mu_{a0}^2 + k^2} + \mu_{a0}\right)},$$

$$h = \sqrt{\frac{3\mu'_{s0}}{2}\left(\sqrt{\mu_{a0}^2 + k^2} - \mu_{a0}\right)},$$

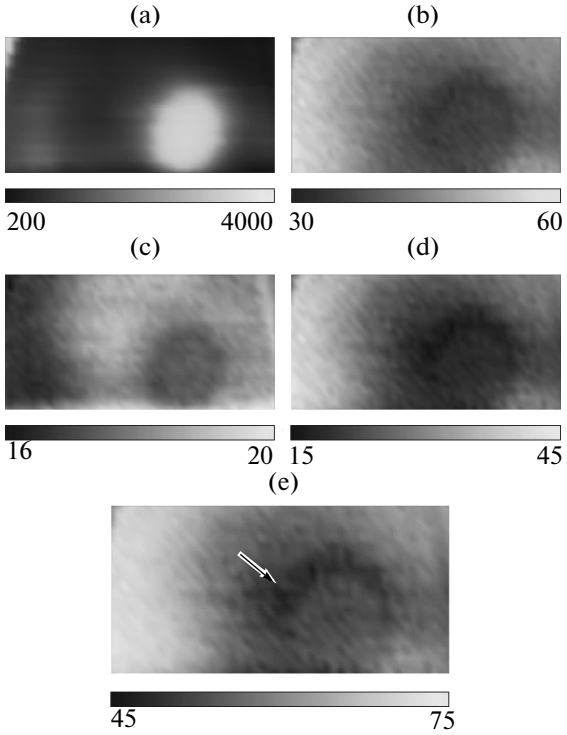

Fig. 2. In vivo DOS imaging of the PLS zone: (a) DOS signal amplitude, arb. un.; (b) total hemoglobin, (c) reduced hemoglobin, and (d) oxyhemoglobin content, μM; (d) blood oxygen saturation, %. Image size, 50 × 70 mm.

where μ'_{s0} and μ_{a0} are transport scattering and absorption indices; $k = 2\pi f/c$ is the wavenumber of the photon density wave in the medium (c is the speed of light in the medium, f is the laser light modulation frequency). These values define the propagation of the photon density wave in the system. The intensity of modulated laser light that has passed through the object is

$$I(\beta, h) \sim I_0 \frac{\exp(-\beta R - ihR)}{R}.$$

Simultaneous solution for β and h yields the scattering and absorption indices $\mu_{a,s}(\lambda_i)$ at each point for three wavelengths. Solving a set of linear equations

$$\mu_a(\lambda_i) = \sum_j (C_j \mu_j(\lambda_i)),$$

we obtain the mean concentrations C_j for HHb, HbO_2, H_2O; the absolute values of extinction coefficients $\mu_j(\lambda_i)$ for these tissue components are well known (http://omlc.ogi.edu/spectra/hemoglobin/).

Morphology and immunohistochemistry. After the DOS scanning, the animals were sacrificed with an i.p. overdose of the anesthetic. The material for histological examination was placed in 10% formalin and stained with hematoxylin/eosin. For IHC the tumor specimens were frozen and stored at −135°C. IHC analysis was performed with a Hypoxyprobe™-1 kit (Hypoxyprobe, USA) in accordance with the recommendations of Natural Pharmacia International. The hypoxia marker pimonidazole (Pim) selectively binds in tissues where the partial oxygen tension does not exceed 10 mmHg. The Pim content and distribution was assessed using monoclonal FITC-labeled antibodies and a laser scanning microscope (LSM 510 META, Carl Zeiss, Germany) with excitation at 488 nm and observation at 500–540 nm.

The DOS outputs were compared with the IHC data, taking into account the results of histological and macroscopic inspection.

RESULTS

The PLS tumor on DOS images of all animals was detected as a region of enhanced signal (Fig. 2a) at all three wavelengths (as compared with the contralateral limb). Numerical reconstruction of component analysis has shown that the HHb concentration was somewhat lowered overall, and declined from the tumor center to the periphery. All tumors had a markedly decreased content of HbO_2 as compared with the surrounding normal tissue. The total Hb content was nonuniformly decreased, just as was the blood oxygen saturation. Figure 2 exemplifies the reconstructed component analysis for a 25-mm PLS.

The DOS results were confirmed by IHC assays. A distinctive feature of PLS was a high fluorescence signal and continuous uniform staining with FITC, indicative of intense Pim binding and low oxygenation of the tumor tissue (Fig. 3a,b).

The RMC-1 tumor, like PLS, was seen on a DOS image as a zone of enhanced signal relative to surrounding tissues. However, numerical reconstruction of component analysis in all cases yielded results essentially different from those for PLS. The HHb concentration in the tumor node projection was evenly decreased. The HbO_2 and tHb indices were uniform and practically the same as in the adjacent normal tissue. The DOS images of RMC-1 revealed high and quite uniform oxygen saturation throughout the tumor. An example of the distribution of the main chromophores in RMC-1 (nodes of ~10 mm) is displayed in Fig. 4. IHC analysis of RMC-1 specimens has revealed only occasional zones of specific Pim binding (Fig. 5), evidencing a high enough oxygenation of these tumors.

DISCUSSION

The results obtained in recent years suggest that neoplasms with low oxygenation are marked by a more aggressive clinical course, higher metastatic potential, poorer survival indices, and refractoriness to therapy [2]. In this context, noninvasive means of assessing the oxygen status of tumor tissue may be important in

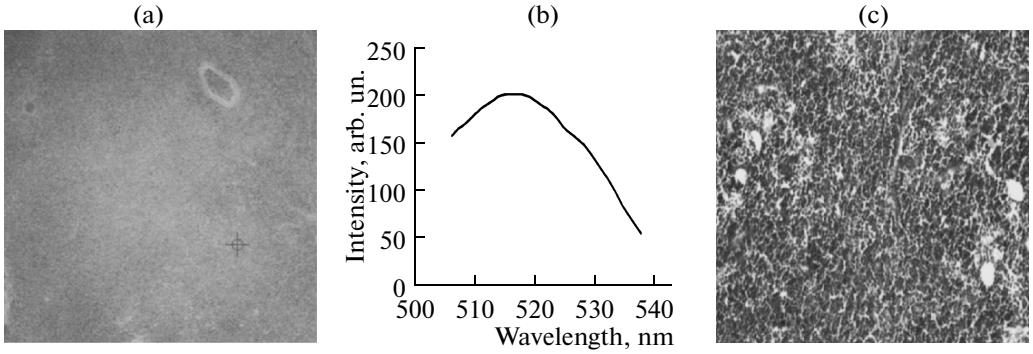

Fig. 3. Microscopic tests for PLS: (a) immunohistochemical staining (×100); (b) spectrum of FITC fluorescence in tumor tissue [site targeted in (a)]; (c) hematoxylin/eosin staining (×100).

prognosticating the disease course and planning the therapy, as well as in monitoring the treatment efficacy.

Estimation of the oxygen status of biological objects by optical methods is based on numerical reconstruction of the component analysis of the tissues. These novel noninvasive methods afford indirect information and, as justly stated [9], must be validated by direct measurements of pO_2 and/or immunohistochemical assays. Here we have used a well-proven IHC assay with pimonidazole to verify the fit of the DOS data to the actual tumor oxygenation level.

The model tumors we have considered differ essentially in their biological properties. The distinctive features of PLS are rapid growth, high cellularity, high mitotic activity, and early necrotization [20]. On the strength of its morphological and physiological properties one could expect low oxygenation and sizable hypoxic zones.

Indeed, DOS imaging of LPS in vivo revealed a markedly lower extent of oxygen saturation relative to surrounding tissues (Fig. 2e). High Pim uptake throughout the tumor found in IHC checks testified to the overall hypoxic state of PLS, despite its appreciable vascularization (Fig. 3). Perhaps the blood supply yet fails to match the demands of the rapidly growing tumor.

In contrast, RMC-1 is a slow-growing epithelial tumor with a developed stromal component and a modest amount of vessels, marked by late emergence of necrotic foci [21]. In these tumors, DOS imaging revealed elevated oxygen saturation on the whole, with a variegated pattern (Fig. 4e). In accord with this, only separate regions accumulating Pim were seen in IHC staining (Fig. 5). Thus, in a slowly growing tumor its vascular bed can satisfy its oxygen demand.

The tHb content in RMC-1 was not appreciably different from that in the surrounding tissues (Fig. 4b), whereas in PLS it was substantially lower (Fig. 2b). These results are consistent with the data [25] showing a positive correlation between the tHb content and blood oxygen saturation in malignancies. There has been a report of elevated total Hb in the region of mammary neoplasms [26]. Our data on the relative decline in tHb versus normal tissue may be explained by high blood filling of the surrounding muscle structures, while the mammary gland is composed largely of adipose tissue with low blood filling.

Thus, here we have demonstrated the possibilities of the DOS technique in assessing the individual metabolic features of a neoplasm. Immunohistochemical

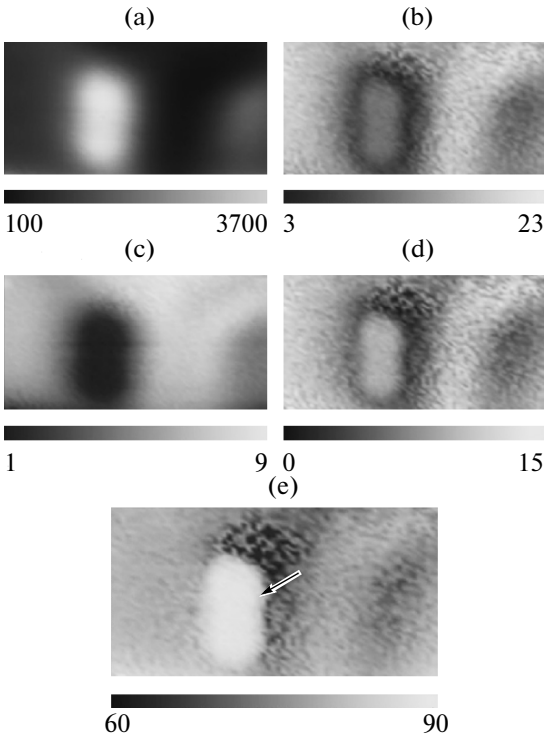

Fig. 4. In vivo DOS imaging of the RMC-1 zone: (a) DOS signal amplitude, arb. un.; (b) total hemoglobin, (c) reduced hemoglobin, and (d) oxyhemoglobin content, μM; (d) blood oxygen saturation, %). Image size, 50 × 70 mm.

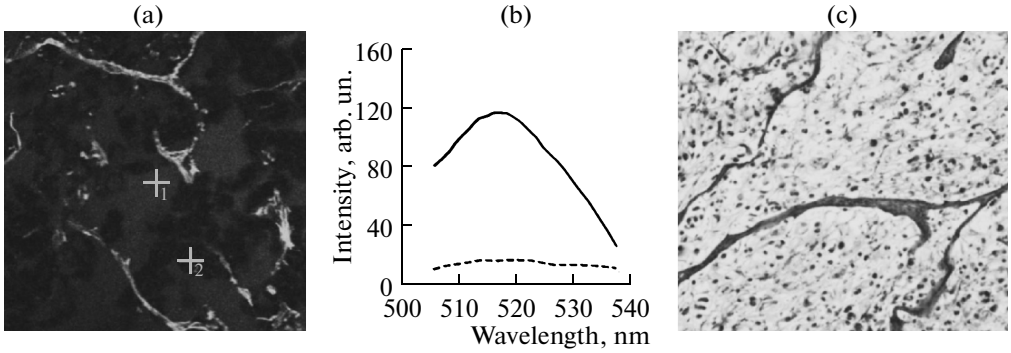

Fig. 5. Microscopic tests for RMC-1: (a) immunohistochemical staining (×100); (b) spectra of FITC fluorescence in tumor tissue [sites marked by crosses in (a)]; (c) hematoxylin/eosin staining (×100).

assays with an exogenous hypoxia marker have confirmed that the DOS output can adequately reflect the oxygen status of the tumor. At the level of the rat model, DOS can already be used in monitoring the efficiency of chemo-, radio-, and photodynamic therapy.

ACKNOWLEDGMENTS

The work was supported by the Russian Foundation for Basic Research (08-02-01042, 09-04-97063) and the RAS Presidium program «Basic Science for Medicine».

REFERENCES

1. J. E. Eriksen and M. R. Horsman, Radiother. Oncol. **81** (2), 119 (2006).
2. P. Vaupel, The Oncologist **13** (3), 21 (2008).
3. M. Hockel, K. Schlenger, B. Aral, et al., Cancer Res. **56**, 4509 (1996).
4. D. M. Brizel, S. P. Scully, J. M. Harrelson, et al., Cancer Res. **56**, 941 (1996).
5. M. Nordsmark, M. Overgaard, and J. Overgaard, Radiother. Oncol. **41** (1), 31 (1996).
6. P. Vaupel, A. Mayer, S. Briest, and M. Hockel, Cancer Res. **63**, 7634 (2003).
7. D. K. Kelleher, O. Thews, and P. Vaupel, Radiother. Oncol. **45** (2), 191 (1997).
8. A. Yaromina, D. Zips, H. D. Thames, et al., Radiother. Oncol. **81** (2), 122 (2006).
9. I. Serganova, J. Humm, C. Ling, and R. Blasberg, Clin. Cancer Res. **12**, 5260 (2006).
10. S. Davda and T. Bezabeh, Cancer Metastasis Rev. **25**, 469 (2006).
11. M. Elas, B. B. Williams, A. Parasca, et al., Magn. Reson. Med. **49**, 682 (2003).
12. V. Ntziachristos and B. Chance, Br. Cancer Res. **3**, 41 (2001).
13. C. Menon, G. M. Polin, I. Prabakaran, et al., Cancer Res. **63**, 7232 (2003).
14. A. Torricelli, L. Spinelli, A. Pifferi, Optics Express **11**, 853 (2003).
15. D. A. Zimnyakov and V. V. Tuchin, Kvant. Elektron. **32**, 849 (2002).
16. S. Kukreti, A. E. Cerussi, W. Tanamai, et al., Radiology **254** (1), 277 (2010).
17. B. J. Tromberg, B. W. Pogue, K. D. Paulsen, Med. Phys. **35**, 2443 (2008).
18. K. Vishwanath, D. Klein, K. Chang, et al., J. Biomed. Optics **14**, 054051-1 (2009).
19. B. W. Pogue, S. P. Poplack, T. O. McBride, et al., Radiology **218** (1), 261 (2001).
20. B. B. Pliss, Byul. Eksperim. Biol. Med. **2**, 95 (1961).
21. V. P. Konoplev and N. D. Lagova, Byul. Eksperim. Biol. Med. **50** (7), 79 (1960).
22. A. G. Orlova, I. V. Turchin, V. I. Plehanov, et al., Laser Phys. Lett. **5** (4), 321 (2008).
23. S. T. Flock, S. L. Jacques, B. C. Wilson, et al., Lasers Surg. Med. **12**, 510 (1992).
24. H. G. van Staveren, C. J. M. Moes, J. van Marle, et al., Appl. Opt. **30**, 4507 (1991).
25. J. Q. Brown, L. G. Wilke, J. Geradts, et al., Cancer Res. **69**, 2919 (2009).
26. S. Srinivasan, B. W. Pogue, B. Brooksby, et al., Technol. Cancer Res. Treatm. **4**, 513 (2005).